PLOS ONE

RESEARCH ARTICLE

Homogeneous-Heterogeneous Reactions in Peristaltic Flow with Convective Conditions

Tasawar Hayat[1,2], Anum Tanveer[1], Humaira Yasmin[1]*, Ahmed Alsaedi[2]

1. Department of Mathematics, Quaid-I-Azam University, Islamabad, Pakistan, **2.** NAAM Research Group, Department of Mathematics, King Abdulaziz University, Jeddah, Saudi Arabia

*qau2011@gmail.com

Abstract

This article addresses the effects of homogeneous-heterogeneous reactions in peristaltic transport of Carreau fluid in a channel with wall properties. Mathematical modelling and analysis have been carried out in the presence of Hall current. The channel walls satisfy the more realistic convective conditions. The governing partial differential equations along with long wavelength and low Reynolds number considerations are solved. The results of temperature and heat transfer coefficient are analyzed for various parameters of interest.

Citation: Hayat T, Tanveer A, Yasmin H, Alsaedi A (2014) Homogeneous-Heterogeneous Reactions in Peristaltic Flow with Convective Conditions. PLoS ONE 9(12): e113851. doi:10.1371/journal.pone.0113851

Editor: Sanjoy Bhattacharya, Bascom Palmer Eye Institute, University of Miami School of Medicine, United States of America

Received: July 11, 2014

Accepted: November 2, 2014

Published: December 2, 2014

Data Availability: The authors confirm that all data underlying the findings are fully available without restriction. All relevant data are within the paper.

Funding: The authors have no support or funding to report.

Competing Interests: The authors have declared that no competing interests exist.

Introduction

In the last few decades, the peristaltic motion of non-Newtonian fluids is a topic of major contemporary interest both in engineering and biological applications. To be more specific, such motion occurs in powder technology, fluidization, chyme movement in the gastrointestinal tract, vasomotion of small blood vessels, locomotion of worms, gliding motility of bacteria, passage of urine from kidney to bladder, reproductive tracts, corrosive and sanitary fluids transport, roller, finger and hose pumps and blood pump through heart lung machine. There is no doubt that viscoelasticity has key role mostly in all the aforementioned applications. Viscoelastic materials are non-Newtonian and possess both the viscous and elastic properties. Most of the biological liquids such as blood at low shear rate, chyme, food bolus etc. are viscoelastic in nature. Another aspect which has yet not been properly addressed is the interaction of rheological characteristics of fluids in peristalsis with convective effects. The significance of convective heat exchange with peristalsis cannot be under estimated for instance in translocation of water in tall trees, dynamic of lakes, solar ponds, lubrication and drying technologies, diffusion of nutrients out of blood, oxygenation, hemodialysis and nuclear reactors. The heat and mass transfer effects in such processes have prominent role.

The magnetohydrodynamic (MHD) character of fluid especially in physiological and industrial processes seems too much important. Such consideration is useful for blood pumping and magnetic resonance imaging (MRI), cancer therapy, hyperthermia etc. The controlled application of low intensity and frequency pulsating fields modify the cell and tissue behavior. Magnetically susceptible of chyme is satisfied from the heat generated by magnetic field or the ions contained in the chyme. Also the magnetotherapy is an application of magnets to human body which is used for the treatment of diseases. The magnets could heal inflammations, ulceration, several diseases of bowel (intestine) and uterus. With all such motivations in mind, the recent researchers are engaged in the development of model of peristalsis of non-Newtonian liquids through different aspects including heat/mass transfer, MHD etc. Few representative attempts in this direction can be mentioned through the recent researchers [1–13] and several studies therein.

To our knowledge, no study has been undertaken yet to discuss the effects of homogeneous-heterogeneous reactions in peristaltic flows of non-Newtonian fluids. Even such study is yet not presented for the viscous fluid. However such consideration is quite important because many chemically reacting systems involve both homogeneous and heterogeneous reactions, with examples occurring in combustion, biochemical systems, catalysis, crops damaging through freezing, cooling towers, fog dispersion, hydrometallurgical processes etc. Hence the main objective of present investigation is to model and analyze the peristalsis of Carreau fluid in a compliant wall channel with convective conditions and homogeneous-heterogeneous reactions. Effects of Hall current and viscous dissipation are also considered. The resulting mathematical systems are solved and examined in the case of long wavelength and small Reynolds number. This article is structured as follows. Section two consists of mathematical modelling and solution expressions up to first order. The behaviors of sundry variables on the temperature, heat transfer coefficient and concentration are discussed graphically in section three. Main results of present study are also included in this section.

Mathematical Formulation

Consider the peristaltic transport of an incompressible Carreau fluid in two-dimensional compliant wall channel. The channel walls satisfy the convective conditions. The Cartesian coordinates x and y are considered along and transverse to the direction of fluid flow respectively. The flow is generated by the peristaltic wave of speed c travelling along the channel walls. The Hall effects are also considered in the flow analysis. Further we consider the flow in the presence of a simple homogeneous and heterogeneous reaction model. There are two chemical species $\bar{A}$ and $\bar{B}$ with concentrations $\bar{a}$ and $\bar{b}$ respectively. The physical model of the wall surface can be analyzed by the expression:

$$y = \pm\eta(x,t) = d + a\sin\frac{2\pi}{\lambda}(x - ct), \tag{1}$$

where a represents the wave amplitude, λ the wavelength, d the half width of symmetric channel, t the time, η displacement of upper wall and $-\eta$ displacement of lower wall.

Consider the uniform magnetic field in the form

$$\mathbf{B}_0=(0,0,B_0). \tag{2}$$

Application of generalized Ohm's law leads to the following expression

$$\mathbf{J}=\sigma\left[\mathbf{V}\times\mathbf{B}_0-\frac{1}{e\breve{n}}(\mathbf{J}\times\mathbf{B}_0)\right], \tag{3}$$

where $\mathbf{J}$ represents the current density, σ the electrical conductivity, $\mathbf{V}$ the velocity field, e the electric charge and $\breve{n}$ the number density of electrons. Also the effects of electric field are considered absent i.e. $\mathbf{E}=0$.

If $\mathbf{V}=[u,\upsilon,0]$ is the velocity with components u *and* υ in the x and y directions respectively then from Eqs. (2) and (3) we have

$$\mathbf{J}\times\mathbf{B}_0=\frac{-\sigma B_0^2}{1+m^2}[(u-m\upsilon),(\upsilon+mu),0], \tag{4}$$

where $m=\dfrac{\sigma B_0}{e\breve{n}}$ serves as the Hall parameter. The reaction model is considered in the form [14–16]:

$$\bar{A}+2\bar{B}\rightarrow 3\bar{B},\quad rate=k_c ab^2,$$

while on the catalyst surface we have the single, isothermal, first order chemical reaction.

$$\bar{A}\rightarrow\bar{B},\quad rate=k_s a,$$

in which k_c and k_s are the rate constants. Both reaction processes are assumed isothermal.

The corresponding flow equations are as follows:

$$\frac{\partial u}{\partial x}+\frac{\partial \upsilon}{\partial y}=0, \tag{5}$$

$$\rho\frac{du}{dt}=-\frac{\partial p}{\partial x}+\frac{\partial R_{xx}}{\partial x}+\frac{\partial R_{xy}}{\partial y}-\frac{\sigma B_0^2}{1+m^2}(u-m\upsilon), \tag{6}$$

$$\rho\frac{d\upsilon}{dt}=-\frac{\partial p}{\partial y}+\frac{\partial R_{yx}}{\partial x}+\frac{\partial R_{yy}}{\partial y}-\frac{\sigma B_0^2}{1+m^2}(\upsilon+mu), \tag{7}$$

$$\rho c_p\frac{dT}{dt}=k\left(\frac{\partial^2 T}{\partial x^2}+\frac{\partial^2 T}{\partial y^2}\right)+R_{xx}\frac{\partial u}{\partial x}+R_{xy}\frac{\partial \upsilon}{\partial x}+R_{yx}\frac{\partial u}{\partial y}+R_{yy}\frac{\partial \upsilon}{\partial y}, \tag{8}$$

$$\frac{da}{dt} = D_A\left(\frac{\partial^2 a}{\partial x^2} + \frac{\partial^2 a}{\partial y^2}\right) - k_c a b^2, \tag{9}$$

$$\frac{db}{dt} = D_B\left(\frac{\partial^2 b}{\partial x^2} + \frac{\partial^2 b}{\partial y^2}\right) + k_c a b^2, \tag{10}$$

where R_{ij} are the components of extra stress tensor for the Carreau fluid and extra stress tensor $\mathbf{R}$ (see refs. [17] and [25]) here is given by

$$\mathbf{R} = [\eta_\infty + (\eta_0 - \eta_\infty)(1 + (\Gamma\dot{\gamma})^2)^{\frac{n-1}{2}}]\dot{\gamma}. \tag{11}$$

Here η_∞ is the infinite shear-rate viscosity, η_0 the zero shear-rate viscosity, Γ the time constant and n the dimensionless form of power law index ($n<1$). Also $\dot{\gamma}$ is defined as follows:

$$\dot{\gamma} = \sqrt{\frac{1}{2}\sum_i \sum_j \dot{\gamma}_{ij}\dot{\gamma}_{ji}} = \sqrt{\frac{1}{2}\Pi}, \tag{12}$$

where Π denotes the second invariant strain tensor defined by $\Pi = tr[\nabla\mathbf{V} + (\nabla\mathbf{V})^t]^2$ and $\dot{\gamma} = \nabla\mathbf{V} + (\nabla\mathbf{V})^t$. Here we consider the case for which $\eta_\infty = 0$ and $\Gamma\dot{\gamma} < 1$. Therefore the extra stress tensor takes the form

$$\mathbf{R} = \eta_0\left(\left(1 + (\Gamma\dot{\gamma})^2\right)^{\frac{n-1}{2}}\right)\dot{\gamma}. \tag{13}$$

It is worth mentioning that the above model reduces to viscous model for $n=1$ or $\Gamma=0$. The component forms of extra stress tensor are

$$R_{xx} = 2\mu_0[1 + \frac{n-1}{2}(\Gamma\dot{\gamma})^2]\frac{\partial u}{\partial x}, \tag{14}$$

$$R_{xy} = \mu_0[1 + \frac{n-1}{2}(\Gamma\dot{\gamma})^2](\frac{\partial u}{\partial y} + \frac{\partial v}{\partial x}) = R_{yx}, \tag{15}$$

$$R_{yy} = 2\mu_0[1 + \frac{n-1}{2}(\Gamma\dot{\gamma})^2]\frac{\partial v}{\partial y}. \tag{16}$$

In above equations $\frac{d}{dt}$ is the material time derivative, ρ the density of fluid, μ_0 the fluid viscosity, v the kinematic viscosity, T the fluid temperature, C the concentration of fluid, T_0 and T_1 the temperatures at the lower and upper walls respectively, K the measure of the strength of homogeneous reaction, D_A and D_B the diffusion coefficients for homogeneous and heterogeneous reactions, c_p the specific heat at constant pressure, k the thermal conductivity, a and b the concentrations of homogeneous and heterogeneous reactions with a_0 serves as uniform concentration of reactant A and k_c the rate constant.

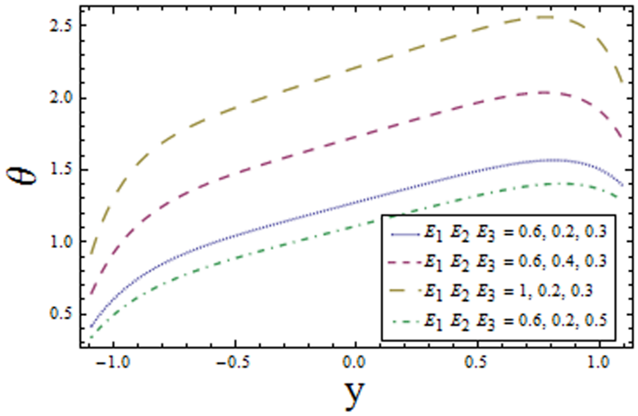

Figure 1. Plot of temperature θ for wall parameters E_1, E_2, E_3, with $\epsilon=0.1$, $t=0.01$, $x=0.2$, $\gamma_1=4$, $\gamma_2=6$, $Br=1$, $m_1=2$, $n=0.4$, $We=0.4$ and $m=0.04$

doi:10.1371/journal.pone.0113851.g001

The exchange of heat at the walls is given by

$$\begin{aligned} k\frac{\partial T}{\partial y} &= -h_1(T-T_1), \text{ at } y=\eta, \\ k\frac{\partial T}{\partial y} &= -h_2(T_0-T), \text{ at } y=-\eta. \end{aligned} \tag{17}$$

Here h_1 and h_2 indicate the heat transfer coefficients at the upper and lower walls respectively.

The no-slip condition at the boundary wall is represented by the following expressions

$$u=0,\ v=\pm\eta_t \text{ at } y=\pm\eta. \tag{18}$$

The compliant wall properties are described through the expression

$$\begin{aligned} &\left[-\tau\frac{\partial^3}{\partial x^3}+m_1^*\frac{\partial^3}{\partial x\partial t^2}+d'\frac{\partial^2}{\partial t\partial x}\right]\eta= \\ &-\rho\frac{du}{dt}+\frac{\partial R_{xx}}{\partial x}+\frac{\partial R_{xy}}{\partial y}-\frac{\sigma B_0^2}{1+m^2}(u-mv) \quad at \quad y=\pm\eta, \end{aligned} \tag{19}$$

in which τ is the elastic tension in the membrane, m_1^* the mass per unit area and d' the coefficient of viscous damping. The mass conditions under the homogeneous and heterogeneous reactions are given through the following expressions:

$$D_A\frac{\partial a}{\partial y}=k_s a, \quad \text{at} \quad y=\pm\eta, \tag{20}$$

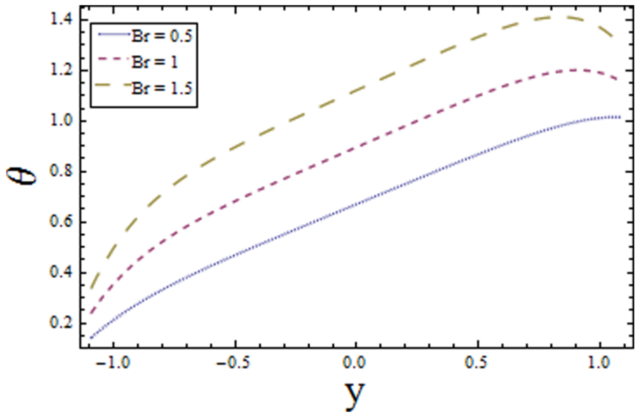

Figure 2. Plot of temperature θ for Brinkman number Br with $\epsilon=0.1,\ t=0.01,\ x=0.2,\ \gamma_1=4,\ \gamma_2=6,\ E_1=0.4,\ E_2=0.2,\ E_3=0.3,\ m_1=2,\ n=0.4,\ We=0.4$ and $m=0.04$

doi:10.1371/journal.pone.0113851.g002

$$D_B\frac{\partial b}{\partial y}=-k_s a, \quad \text{at} \quad y=\pm\eta, \tag{21}$$

where k_s indicates the rate constant.

Performing $\frac{\partial}{\partial y}(6)-\frac{\partial}{\partial x}(7)$ we get

$$\begin{aligned}\rho\frac{d}{dt}\left(\frac{\partial u}{\partial y}-\frac{\partial v}{\partial x}\right)=&\frac{\partial^2 R_{xx}}{\partial y\partial x}-\frac{\partial^2 R_{yx}}{\partial x^2}+\frac{\partial^2 R_{xy}}{\partial y^2}-\frac{\partial^2 R_{yy}}{\partial x\partial y}-\frac{\sigma B_0^2}{1+m^2}\left(\frac{\partial u}{\partial y}-m\frac{\partial v}{\partial y}\right)\\&+\frac{\sigma B_0^2}{1+m^2}\left(\frac{\partial v}{\partial x}+m\frac{\partial u}{\partial x}\right).\end{aligned}\tag{22}$$

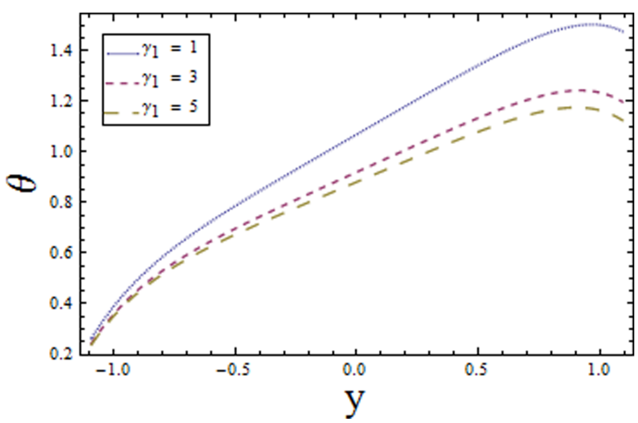

Figure 3. Plot of temperature θ for Biot number γ_1 with $\epsilon=0.1,\ t=0.01,\ x=0.2,\ Br=1,\ \gamma_2=6,\ E_1=0.4,\ E_2=0.2,\ E_3=0.3,\ m_1=2,\ n=0.4,\ We=0.4$ and $m=0.04$

doi:10.1371/journal.pone.0113851.g003

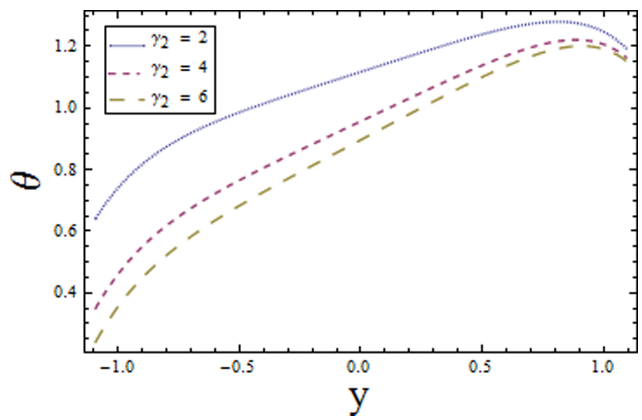

Figure 4. Plot of temperature θ for Biot number γ_2 with $\epsilon=0.1,\ t=0.01,\ x=0.2,\ \gamma_1=4,\ Br=1\ E_1=0.4,\ E_2=0.2,\ E_3=0.3,\ m_1=2,\ n=0.4,\ We=0.4$ and $m=0.04$.

doi:10.1371/journal.pone.0113851.g004

Introducing the stream function $\psi(x,y,t)$ and defining the following dimensionless variables:

$$u=\frac{\partial\psi}{\partial y},\quad \upsilon=-\frac{\partial\psi}{\partial x},$$

$$\psi^*=\frac{\psi}{cd},x^*=\frac{x}{\lambda},y^*=\frac{y}{d},\ t^*=\frac{ct}{\lambda},\ \eta^*=\frac{\eta}{d},\theta=\frac{T-T_0}{T_1-T_0},\hat{\dot{\gamma}}=\frac{d}{c}\dot{\gamma},\xi^*=\frac{D_B}{D_A},$$

$$g^*=\frac{a}{a_0},h^*=\frac{b}{a_0},R^*_{xx}=\frac{\lambda}{\mu_0 c}R_{xx},\ R^*_{xy}=\frac{d}{\mu_0 c}R_{xy},\ R^*_{yx}=\frac{d}{\mu_0 c}R_{yx},R^*_{yy}=\frac{d}{\mu_0 c}R_{yy}. \quad (23)$$

Eqs. (8), (9) and (22) yield

$$\delta Re\left[\frac{d}{dt}\left(\frac{\partial^2\psi}{\partial y^2}+\delta^2\frac{\partial^2\psi}{\partial x^2}\right)\right]=\delta^2\frac{\partial^2 R_{xx}}{\partial y\partial x}-\delta^2\frac{\partial^2 R_{yx}}{\partial x^2}+\frac{\partial^2 R_{xy}}{\partial y^2}+\delta\frac{\partial^2 R_{yy}}{\partial x\partial y} -\frac{m_1^2}{1+m^2}\left(\frac{\partial^2\psi}{\partial y^2}+\delta^2\frac{\partial^2\psi}{\partial x^2}+2m\delta\frac{\partial^2\psi}{\partial x\partial y}\right), \quad (24)$$

$$\delta\,\mathrm{Pr}\,\mathrm{Re}\frac{d\theta}{dt}= \delta^2\frac{\partial^2\theta}{\partial x^2}+\frac{\partial^2\theta}{\partial y^2}+Br\left(\delta^2 R_{xx}\frac{\partial^2\psi}{\partial y^2}-\delta^2 R_{xy}\frac{\partial^2\psi}{\partial x^2}+R_{yx}\frac{\partial^2\psi}{\partial y^2}-\delta^3 R_{yy}\frac{\partial^2\psi}{\partial x\partial y}\right), \quad (25)$$

$$\mathrm{Re}\delta\frac{dg}{dt}=\frac{1}{Sc}\left(\delta^2\frac{\partial^2 g}{\partial x^2}+\frac{\partial^2 g}{\partial y^2}\right)-Kgh^2, \quad (26)$$

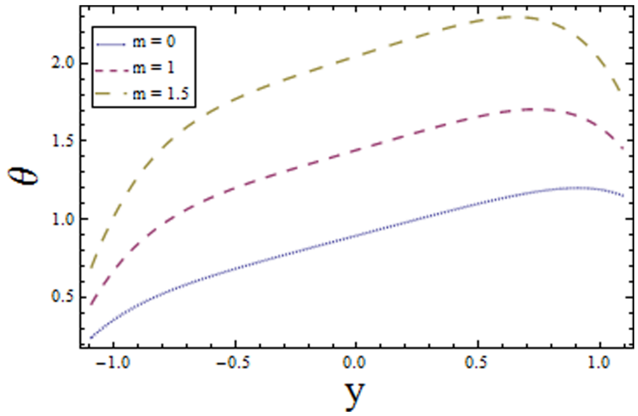

Figure 5. Plot of temperature θ for Hall parameter m with $\epsilon=0.1,\ t=0.01,\ x=0.2,\ \gamma_1=4,\ \gamma_2=6,\ E_1=0.4,\ E_2=0.2,\ E_3=0.3,\ m_1=2,\ n=0.4,\ We=0.4$ **and** $Br=1$.

doi:10.1371/journal.pone.0113851.g005

$$\mathrm{Re}\delta\frac{dh}{dt}=\frac{\xi}{Sc}\left(\delta^2\frac{\partial^2 h}{\partial x^2}+\frac{\partial^2 h}{\partial y^2}\right)+Kgh^2, \tag{27}$$

with the dimensionless conditions

$$\eta\ =\ 1+\epsilon\sin 2\pi(x-t), \tag{28}$$

$$\frac{\partial\theta}{\partial y}+\gamma_1(\theta-1)\ =\ 0\ \ \text{at}\ y=\eta,$$

$$\frac{\partial\theta}{\partial y}-\gamma_2\theta\ =\ 0\ \ \text{at}\ y=-\eta, \tag{29}$$

$$\frac{\partial g}{\partial y}-Mg=0\ \text{at}\ y=\pm\eta, \tag{30}$$

$$\xi\frac{\partial h}{\partial y}+Mh=0\ \text{at}\ y=\pm\eta, \tag{31}$$

$$\boldsymbol{\psi}_y=0\ \ \text{at}\ y=\pm\eta, \tag{32}$$

$$\left[E_1\frac{\partial^3}{\partial x^3}+E_2\frac{\partial^3}{\partial x\partial t^2}+E_3\frac{\partial^2}{\partial x\partial t}\right]\eta=-\mathrm{Re}\delta\frac{d}{dt}(\frac{\partial\boldsymbol{\psi}}{\partial y})+\delta^2\frac{\partial}{\partial x}R_{xx}+\frac{\partial}{\partial y}R_{xy}$$
$$-\frac{m_1^2}{1+m^2}\left(\frac{\partial\boldsymbol{\psi}}{\partial y}+m\delta\frac{\partial\boldsymbol{\psi}}{\partial x}\right)\quad\text{at}\ y=\pm\eta. \tag{33}$$

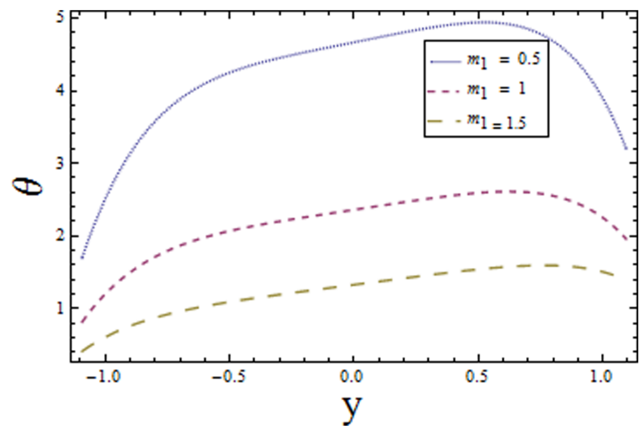

Figure 6. Plot of temperature θ for Hartman number m_1 with $\epsilon=0.1$, $t=0.01$, $x=0.2$, $\gamma_1=4$, $\gamma_2=6$, $E_1=0.4$, $E_2=0.2$, $E_3=0.3$, $Br=1$, $n=0.4$, $We=0.4$ and $m=0.04$.

doi:10.1371/journal.pone.0113851.g006

Also Eqs. (14–16) become

$$R_{xx}= 2(1+\frac{n-1}{2}We^2\widehat{\dot{\gamma}}^2)\boldsymbol{\psi}_{xy}, \tag{34}$$

$$R_{xy}= R_{yx}=2(1+\frac{n-1}{2}We^2\widehat{\dot{\gamma}}^2)(\boldsymbol{\psi}_{yy}-\delta^2\boldsymbol{\psi}_{xx}), \tag{35}$$

$$R_{yy} = -2\delta(1+\frac{n-1}{2}We^2\widehat{\dot{\gamma}}^2)\boldsymbol{\psi}_{xy}. \tag{36}$$

In above equations asterisks have been omitted for simplicity. Here δ is the dimensionless wave number, the Reynolds number Re, the Prandtl number Pr, the

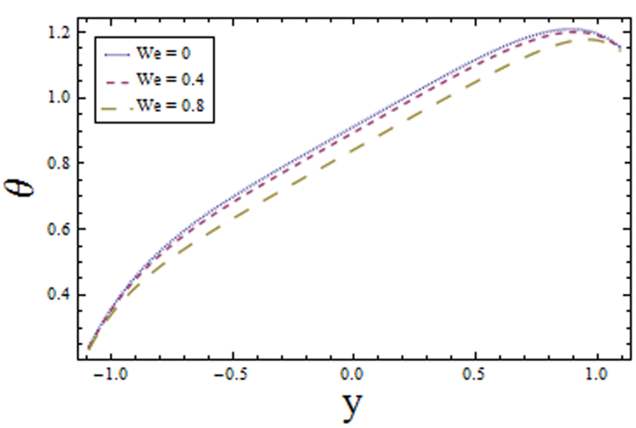

Figure 7. Plot of temperature θ for Weissenberg number We with $\epsilon=0.1$, $t=0.01$, $x=0.2$, $\gamma_1=4$, $\gamma_2=6$, $E_1=0.4$, $E_2=0.2$, $E_3=0.3$, $m_1=2$, $n=0.4$, $Br=1$ and $m=0.04$.

doi:10.1371/journal.pone.0113851.g007

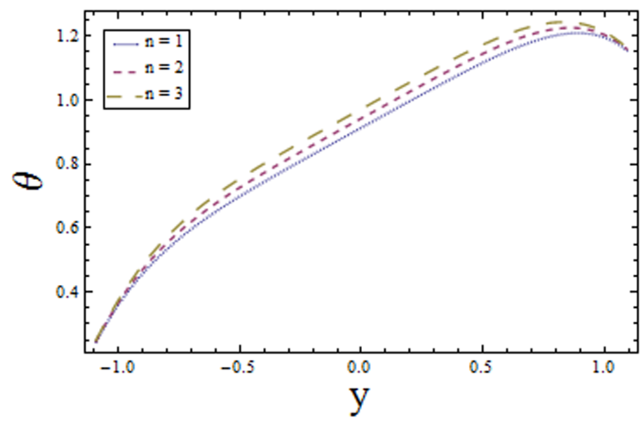

Figure 8. Plot of temperature θ for power law index n with $\epsilon=0.1,\ t=0.01,\ x=0.2,\ \gamma_1=4,\ \gamma_2=6,\ E_1=0.4,\ E_2=0.2,\ E_3=0.3,\ m_1=2,\ We=0.4,\ Br=1$ and $m=0.04$.

doi:10.1371/journal.pone.0113851.g008

amplitude ratio ϵ, the chemical reaction parameter γ, the Hartman number m_1, the non-dimensional elasticity parameters E_1, E_2, E_3, the Schmidt number Sc, the Eckert number E, the Brinkman number Br, the heat transfer Biot numbers γ_1, γ_2, the Weissenberg number We, the ratio of diffusion coefficient ξ, the strength measuring parameters K and M (for homogeneous and heterogeneous reaction respectively) and $\hat{\dot{\gamma}}$ (non-dimensional form of $\dot{\gamma}$) are given through the following variables:

$$
\begin{aligned}
\delta &= \frac{d}{\lambda},\mathrm{Re}=\frac{cd}{\nu},\ \mathrm{Pr}=\frac{\mu c_p}{k},\epsilon=\frac{a}{d},We=\frac{\Gamma c}{d},E=\frac{c^2}{(T_1-T_0)c_p},\\
Sc &= \frac{\mu_0}{\rho D_A},E_1=-\frac{\tau d^3}{\lambda^3\mu_0 c},E_2=\frac{m_1^* c d^3}{\lambda^3\mu_0},E_3=\frac{d^3 d'}{\mu\lambda^2},Br=EPr,\\
\hat{\dot{\gamma}} &= \sqrt{4\delta^2\left(\frac{\partial^2\psi}{\partial x\partial y}\right)^2+\left(\frac{\partial^2\psi}{\partial y^2}-\delta^2\frac{\partial^2\psi}{\partial x^2}\right)},\gamma_1=\frac{h_1 d}{k},\gamma_2=\frac{h_2 d}{k},\\
m_1^2 &= \frac{\sigma B_0^2 d^2}{\mu_0},\xi=\frac{D_B}{D_A},K=\frac{k_c a_0^2 d^2}{\nu},M=\frac{k_s d}{D_A}.
\end{aligned}
\tag{37}
$$

We now employ the approximations of long wavelength and low Reynolds number [17–23] and equality of diffusion coefficients D_A and D_B i.e. $\xi=1$. The assumption $\xi=1$ leads to the following relation:

$$g(\eta)+h(\eta)=1, \tag{38}$$

and we obtain the following set of equations

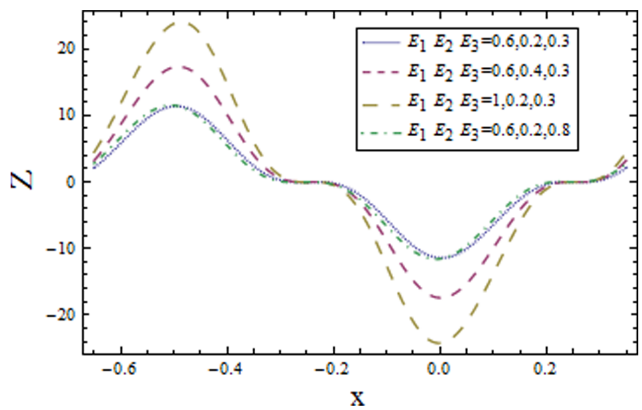

Figure 9. Plot of heat transfer coefficient Z for wall parameters E_1, E_2, E_3, with $\epsilon=0.1$, $t=0.01$, $\gamma_1=4$, $\gamma_2=6$, $m_1=2$, $We=0.4$, $n=0.4$, $Br=1$ and $m=0.04$.

doi:10.1371/journal.pone.0113851.g009

$$\frac{\partial^4\psi}{\partial y^4}+\frac{3}{2}(n-1)We^2\frac{\partial^4\psi}{\partial y^4}\left(\frac{\partial^2\psi}{\partial y^2}\right)^2 +3(n-1)We^2\left(\frac{\partial^3\psi}{\partial y^3}\right)^2\frac{\partial^2\psi}{\partial y^2}-\frac{m_1^2}{1+m^2}\frac{\partial^2\psi}{\partial y^2}=0, \tag{39}$$

$$\frac{\partial^2\theta}{\partial y^2}+Br\left(\frac{\partial^2\psi}{\partial y^2}\right)^2\left(1+\frac{n-1}{2}We^2\left(\frac{\partial^2\psi}{\partial y^2}\right)^2\right)=0, \tag{40}$$

$$\frac{1}{Sc}\frac{\partial^2 g}{\partial y^2}-Kg(1-g)^2=0, \tag{41}$$

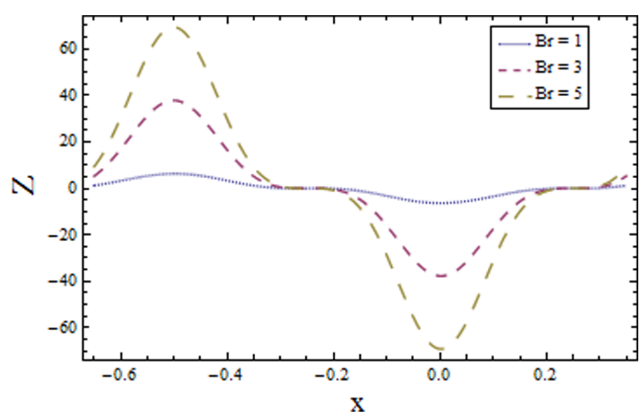

Figure 10. Plot of heat transfer coefficient Z for Brinkman number Br with $\epsilon=0.1$, $t=0.01$, $\gamma_1=4$, $\gamma_2=6$, $E_1=0.4$, $E_2=0.2$, $E_3=0.3$, $m_1=2$, $n=0.4$, $We=0.4$ and $m=0.04$.

doi:10.1371/journal.pone.0113851.g010

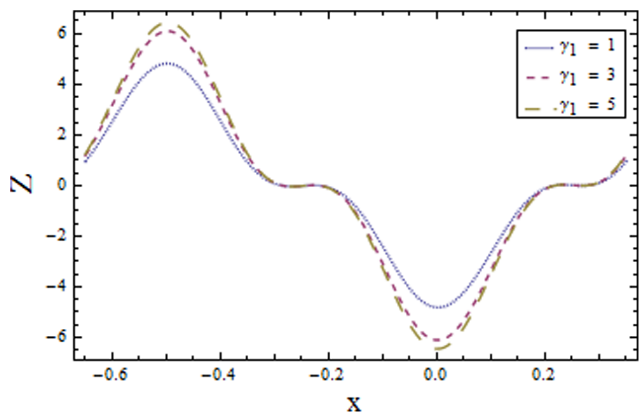

Figure 11. Plot of heat transfer coefficient Z for Biot number γ_1 with $\epsilon=0.1,\ t=0.01,\ Br=1,\ \gamma_2=6,\ E_1=0.4,\ E_2=0.2,\ E_3=0.3,\ m_1=2,\ n=0.4,\ We=0.4$ and $m=0.04$.

doi:10.1371/journal.pone.0113851.g011

$$\frac{\partial \psi}{\partial y} = 0 \text{ at } y=\pm\eta, \tag{42}$$

$$\begin{aligned} \frac{\partial \theta}{\partial y}+\gamma_1(\theta-1) &= 0, \text{ at } y=\eta, \\ \frac{\partial \theta}{\partial y}-\gamma_2\theta &= 0, \text{ at } y=-\eta, \end{aligned} \tag{43}$$

$$\frac{\partial g}{\partial y}-Mg = 0, \text{ at } y=\pm\eta, \tag{44}$$

$$\begin{aligned} \left[E_1\frac{\partial^3}{\partial x^3}+E_2\frac{\partial^3}{\partial x\partial t^2}+E_3\frac{\partial^2}{\partial x\partial t}\right]\eta &= \frac{\partial^3\psi}{\partial y^3}+\frac{3}{2}(n-1)We^2\left(\frac{\partial^2\psi}{\partial y^2}\right)^2\frac{\partial^3\psi}{\partial y^3} \\ &\quad -\frac{m_1^2}{1+m^2}\frac{\partial\psi}{\partial y} \text{ at } y = \pm\eta. \end{aligned} \tag{45}$$

2.1 Method of solution

It is seen from Eqs. (39) and (41) that these Eqs. are non-linear and involve Weissenberg number We and homogeneous reaction parameter K respectively. Therefore the problem at hand cannot be solved exactly, but can be linearized about "small" parameter to the mathematical description of the exactly solvable problem. The technique is referred as perturbation. Perturbation method represent a very powerful tool in modern mathematical physics and, in particular, in fluid dynamics and leads to a series solution of resulting system of equations having small paramter. Therefore we have applied this method to form the series

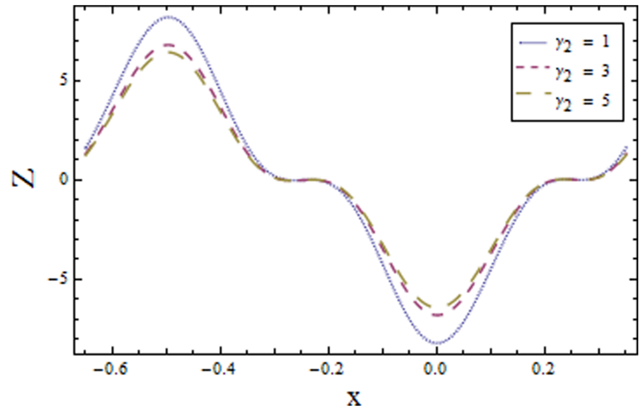

Figure 12. Plot of heat transfer coefficient Z for Biot number γ_2 with $\epsilon=0.1,\ t=0.01,\ \gamma_1=4,\ Br=1,\ E_1=0.4,\ E_2=0.2,\ E_3=0.3,\ m_1=2,\ n=0.4,\ We=0.4$ and $m=0.04$.

doi:10.1371/journal.pone.0113851.g012

solutions for stream function ψ, temperature θ and concentration g corresponding to the involved non-linear quantities (We and K). For this we write the flow quantities in the forms:

$$\psi=\psi_0+We^2\psi_1+O\left(We^4\right),$$

$$\theta=\theta_0+We^2\theta_1+O\left(We^4\right),$$

$$g=g_0+Kg_1+O\left(K^2\right),$$

$$Z=Z_0+We^2Z_1+O(We^4).$$

2.2 Zeroth order system and its solution

The zeroth order system is given by

$$\frac{\partial^4\psi_0}{\partial y^4}-\frac{m_1^2}{1+m^2}\frac{\partial^2\psi_0}{\partial y^2}\ =\ 0, \tag{46}$$

$$\frac{\partial^2\theta_0}{\partial y^2}+Br\left(\frac{\partial^2\psi_0}{\partial y^2}\right)^2\ =\ 0, \tag{47}$$

$$\frac{1}{Sc}\frac{\partial^2 g_0}{\partial y^2}=0, \tag{48}$$

$$\frac{\partial\psi_0}{\partial y}=0,\qquad \text{at } y=\pm\eta, \tag{49}$$

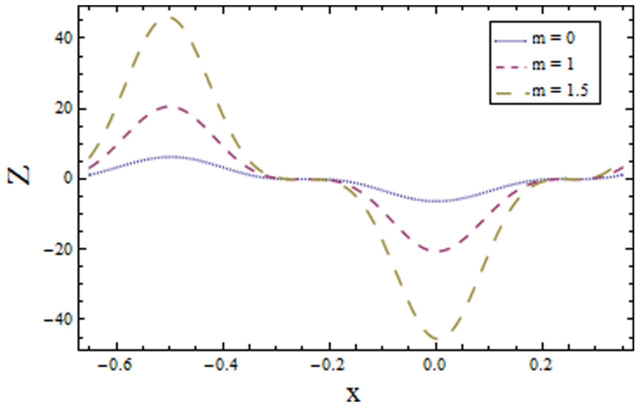

Figure 13. Plot of heat transfer coefficient Z for Hall parameter m with $\epsilon=0.1,\ t=0.01,\ \gamma_1=4,\ \gamma_2=6,$ $E_1=0.4,\ E_2=0.2,\ E_3=0.3,\ m_1=2,\ n=0.4,\ We=0.4$ and $Br=1$.

doi:10.1371/journal.pone.0113851.g013

$$\frac{\partial \theta_0}{\partial y}+\gamma_1(\theta_0-1)=0 \quad \text{at} \quad y=\eta,$$

$$\frac{\partial \theta_0}{\partial y}-\gamma_2\theta_0=0 \quad \text{at} \quad y=-\eta, \tag{50}$$

$$\frac{\partial g_0}{\partial y}-Mg_0=0, \quad \text{at } y=\pm\eta, \tag{51}$$

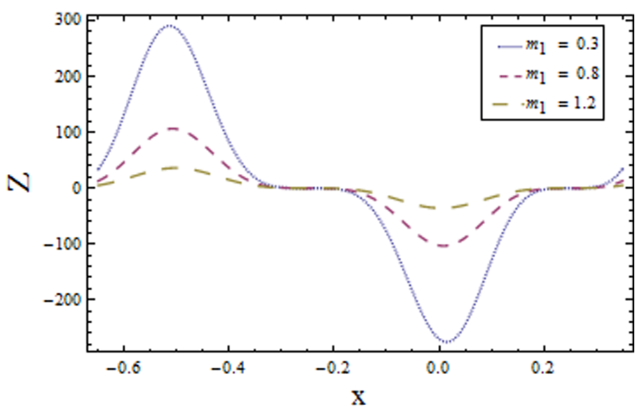

Figure 14. Plot of heat transfer coefficient Z for Hartman number m_1 with $\epsilon=0.1,\ t=0.01,\ \gamma_1=4,\ \gamma_2=6,$ $E_1=0.4,\ E_2=0.2,\ E_3=0.3,\ Br=1,\ n=0.4,\ We=0.4$ and $m=0.04$.

doi:10.1371/journal.pone.0113851.g014

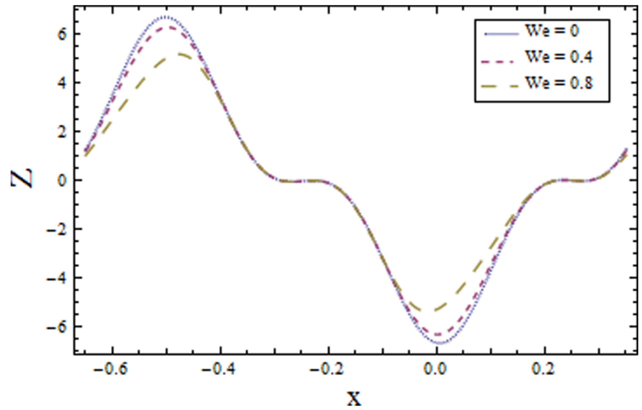

Figure 15. Plot of heat transfer coefficient Z for Weissenberg number We with $\epsilon=0.1$, $t=0.01$, $\gamma_1=4$, $\gamma_2=6$, $E_1=0.4$, $E_2=0.2$, $E_3=0.3$, $m_1=2$, $n=0.4$, $Br=1$ and $m=0.04$.

doi:10.1371/journal.pone.0113851.g015

$$\left[E_1\frac{\partial^3}{\partial x^3}+E_2\frac{\partial^3}{\partial x\partial t^2}+E_3\frac{\partial^2}{\partial x\partial t}\right]\eta=\frac{\partial^3\psi_0}{\partial y^3}-\frac{m_1^2}{1+m^2}\frac{\partial\psi_0}{\partial y}\quad \text{at } y=\pm\eta. \tag{52}$$

The solutions of Eqs. (46–48) subject to the boundary conditions (49–52) are

$$\psi_0=A_2(\sqrt{H}y-\operatorname{sech}(\sqrt{H}\eta)\sinh(\sqrt{H}y)), \tag{53}$$

$$\theta_0=-L_4+\frac{4L_5}{H}y^2-\frac{(L_4\gamma_2-L_2)}{1+\gamma_2\eta}y-\frac{2L_5\cosh(2\sqrt{H}y)}{H^2}, \tag{54}$$

$$g_0=B_1+B_2y, \tag{55}$$

$$\begin{aligned}Z_0&=\eta_x\theta_{0y}(\eta),\\ &=\eta_x\Big[\frac{-4L_5(-2\sqrt{H}\eta+\sinh(2\sqrt{H}\eta))}{H^{3/2}}-\frac{L_4\gamma_2}{1+\gamma_2\eta}\\ &\quad-\frac{2L_5(-2H\eta(2+\gamma_2\eta)+\gamma_2\cosh(2\sqrt{H}\eta)+2\sqrt{H}\sinh(2\sqrt{H}\eta))}{H^2(1+\gamma_2\eta)}\Big].\end{aligned} \tag{56}$$

2.3 First order system and its solution

At this order we have

$$\frac{\partial^4\psi_1}{\partial y^4}+\frac{3}{2}(n-1)\frac{\partial^4\psi_0}{\partial y^4}\left(\frac{\partial^2\psi_0}{\partial y^2}\right)^2+3(n-1)\left(\frac{\partial^3\psi_0}{\partial y^3}\right)^2\frac{\partial^2\psi_0}{\partial y^2}-\frac{m_1^2}{1+m^2}\frac{\partial^2\psi_1}{\partial y^2}=0, \tag{57}$$

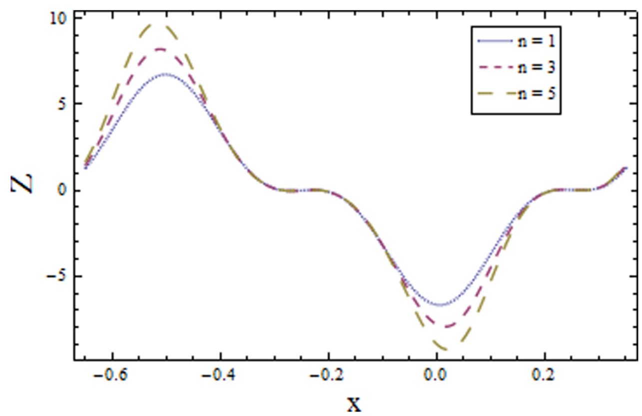

Figure 16. Plot of heat transfer coefficient Z for power law index n with $\epsilon=0.1,\ t=0.01,\ \gamma_1=4,\ \gamma_2=6,\ E_1=0.4,\ E_2=0.2,\ E_3=0.3,\ m_1=2,\ Br=1,\ We=0.4$ and $m=0.04$.

doi:10.1371/journal.pone.0113851.g016

$$\frac{\partial^2\theta_1}{\partial y^2}+2Br\frac{\partial^2\boldsymbol{\psi}_0}{\partial y^2}\frac{\partial^2\boldsymbol{\psi}_1}{\partial y^2}+\frac{Br(n-1)}{2}\left(\frac{\partial^2\boldsymbol{\psi}_0}{\partial y^2}\right)^4=0, \tag{58}$$

$$\frac{1}{Sc}\frac{\partial^2 g_1}{\partial y^2}-g_0(1-g_0)^2=0, \tag{59}$$

$$\frac{\partial\boldsymbol{\psi}_1}{\partial y}=0,\ \text{at}\ y=\pm\eta, \tag{60}$$

$$\frac{\partial\theta_1}{\partial y}+\gamma_1\theta_1=0\ \text{at}\ \ y=\eta,$$

$$\frac{\partial\theta_1}{\partial y}-\gamma_2\theta_1=0\ \text{at}\ \ y=-\eta, \tag{61}$$

$$\frac{\partial g_1}{\partial y}-Mg_1=0,\ \ \text{at}\ y=\pm\eta, \tag{62}$$

$$\frac{\partial^3\boldsymbol{\psi}_1}{\partial y^3}+\frac{3}{2}(n-1)\frac{\partial^3\boldsymbol{\psi}_0}{\partial y^3}\left(\frac{\partial^2\boldsymbol{\psi}_0}{\partial y^2}\right)^2-\frac{m_1^2}{1+m^2}\frac{\partial\boldsymbol{\psi}_1}{\partial y}=0\ \ \text{at}\ y=\pm\eta. \tag{63}$$

Solving Eqs. (57–59) and then applying the corresponding boundary conditions we get the solutions in the forms given below:

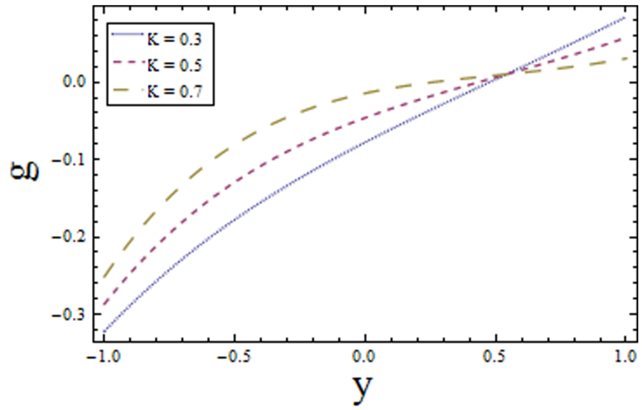

Figure 17. Plot of concentration g for homogeneous reaction parameter K with $\epsilon=0.2,\ t=0.1,\ x=0.1,$ $Sc=1.5$ and $M=2$.

doi:10.1371/journal.pone.0113851.g017

$$\begin{aligned}\psi_1 = {} & A_3A_4\exp(-\sqrt{H}(3y+2\eta))[-3\exp(2\sqrt{H}y)+3\exp(4\sqrt{H}y)\\ & +\exp(2\sqrt{H}\eta)+\exp(4\sqrt{H}\eta)-\exp(2\sqrt{H}(3y+\eta))\\ & -\exp(2\sqrt{H}(3y+2\eta))-3\exp(2\sqrt{H}(y+3\eta))\\ & +3\exp(2\sqrt{H}(2y+3\eta))+12(\sqrt{H}(y-\eta)-1)\exp(4\sqrt{H}(y+\eta))\\ & +12(\sqrt{H}(y-\eta)+1)\exp(2\sqrt{H}(y+\eta))\\ & +12(\sqrt{H}(y+\eta)-1)\exp(2\sqrt{H}(2y+\eta))\\ & +12(\sqrt{H}(y+\eta)+1)\exp(2\sqrt{H}(y+2\eta))],\end{aligned} \tag{64}$$

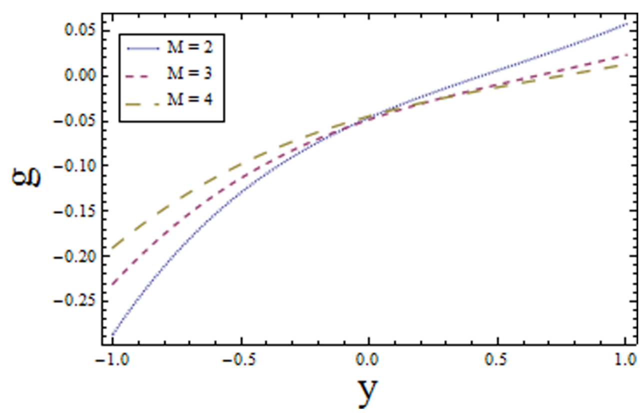

Figure 18. Plot of concentration g for heterogeneous reaction parameter M with $\epsilon=0.2,\ t=0.1,\ x=0.1,$ $Sc=1.5$ and $K=0.5$.

doi:10.1371/journal.pone.0113851.g018

$$
\begin{aligned}
\theta_1 = {} & L_6 \exp(-4\sqrt{H}(y+\eta))[(9Br-4)L_1\{\exp(4\sqrt{H}\eta)+\exp(6\sqrt{H}\eta) \\
& +\exp(4\sqrt{H}(2y+\eta))+\exp(2\sqrt{H}(4y+3\eta))\}-12BrL_1\{\exp(2\sqrt{H}(y+\eta)) \\
& +\exp(2\sqrt{H}(3y+\eta))+\exp(2\sqrt{H}(y+4\eta))+\exp(2\sqrt{H}(3y+4\eta))\} \\
& +4L_1\exp(2\sqrt{H}(y+2\eta))(16+3Br(-3+4\sqrt{H}(y-\eta)) \\
& -4L_1\exp(6\sqrt{H}(y+\eta))(-16+3Br(3+4\sqrt{H}(y-\eta)) \\
& +\exp(4\sqrt{H}y)\{(4+3Br)L_1-4(3Br-4)\sqrt{H}(y(\gamma_1-\gamma_2)-\eta(\gamma_1+\gamma_2)-2)\} \\
& +\exp(2\sqrt{H}(2y+5\eta))\{(4+3Br)L_1+4(3Br-4)\sqrt{H}(y(\gamma_1-\gamma_2)-\eta(\gamma_1+\gamma_2)-2))\} \\
& +4L_1\exp(2\sqrt{H}(y+3\eta))(16+3Br(4\sqrt{H}(y+\eta)-3)) \\
& -4L_1\exp(2\sqrt{H}(3y+2\eta))(-16+3Br(4\sqrt{H}(y+\eta)+3)) \\
& +\exp(4\sqrt{H}(y+2\eta))\{3(9Br-20)L_1-28(3Br-4)\sqrt{H}(y(\gamma_1-\gamma_2)-\eta(\gamma_1+\gamma_2)-2) \\
& +48BrH(L_1y^2+2y(\gamma_1-\gamma_2)\eta-4\eta-3\eta^2(\gamma_1+\gamma_2)-2\gamma_1\gamma_2\eta^3)\} \\
& +\exp(2\sqrt{H}(2y+\eta))\{3(9Br-20)L_1+28(3Br-4)\sqrt{H}(y(\gamma_1-\gamma_2)-\eta(\gamma_1+\gamma_2)-2) \\
& +48BrH(L_1y^2+2y(\gamma_1-\gamma_2)\eta-4\eta-3\eta^2(\gamma_1+\gamma_2)-2\gamma_1\gamma_2\eta^3)\} \\
& +16\exp(2\sqrt{H}(2y+3\eta))\{(3Br-4)L_1+2\sqrt{H}((4-3Br)(y(\gamma_1+\gamma_2)-2) \\
& +2(3Br-2)+\eta(\gamma_1+\gamma_2)+6Br\gamma_1\gamma_2\eta^2) \\
& +12BrH^{3/2}\eta(2y\eta(\gamma_2-\gamma_1)-L_1y^2+\eta(4+3\eta(\gamma_1+\gamma_2)+2\gamma_1\gamma_2\eta^2)) \\
& +12H((-1+Br)L_1y^2+(Br-2)(\gamma_1-\gamma_2)y\eta+4\eta+3\eta^2(\gamma_1+\gamma_2) \\
& +2\gamma_1\gamma_2\eta^3-2\eta Br(1+\gamma_1\eta)(1+\gamma_2\eta))\}-16\exp(4\sqrt{H}(y+\eta))\{(4-3Br)L_1 \\
& -2\sqrt{H}((3Br-4)(y(\gamma_1-\gamma_2)-2)-2\eta(3Br-2)(\gamma_1+\gamma_2)-6Br\gamma_1\gamma_2\eta^2) \\
& -12H((Br-1)L_1y^2+\eta(\gamma_1-\gamma_2)(Br-2)y+4\eta+3\eta^2(\gamma_1+\gamma_2)+2\gamma_1\gamma_2\eta^3 \\
& -2\eta Br(1+\gamma_1\eta)(1+\gamma_2\eta))+12BrH^{3/2}\eta(2y\eta(\gamma_2-\gamma_1)-L_1y^2 \\
& +4\eta+3\eta^2\gamma_2+\gamma_1\eta^2(3+2\eta\gamma_2)\}],
\end{aligned}
\tag{65}
$$

$$
g_1 = H_1 + C_1y + C_2y^2 + C_3y^3 + C_4y^4 + C_5y^5, \tag{66}
$$

and the heat transfer coefficient is

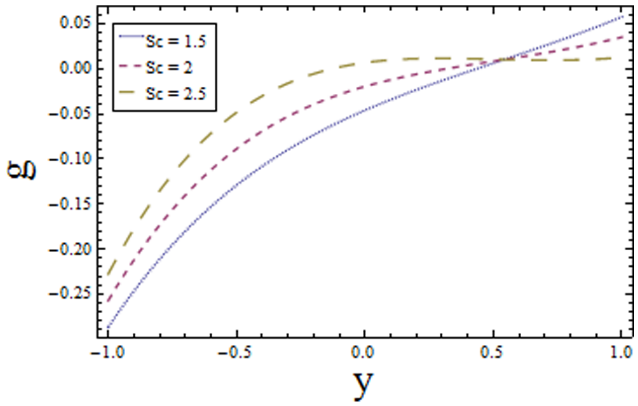

Figure 19. Plot of concentration g for Schmidt number Sc with $\epsilon=0.2,\ t=0.1,\ x=0.1\ K=0.5$ and $M=2.$

doi:10.1371/journal.pone.0113851.g019

$$\begin{aligned} Z_1 &= \eta_x \theta_{1y}(\eta), \\ &= \eta_x L_7[-4(1+\exp(2\sqrt{H}\eta)(8\exp(2\sqrt{H}\eta)-8\exp(6\sqrt{H}\eta) \\ &\quad + \exp(8\sqrt{H}\eta)+24\sqrt{H}\eta\exp(4\sqrt{H}\eta)-1) \\ &\quad +3Br\{\exp(10\sqrt{H}\eta)-1+(\exp(8\sqrt{H}\eta)+\exp(2\sqrt{H}\eta))(8\sqrt{H}\eta-7) \\ &\quad -8\exp(6\sqrt{H}\eta)(1-2\sqrt{H}\eta+4H\eta^2)+8\exp(4\sqrt{H}\eta)(1+2\sqrt{H}\eta+4H\eta^2)\}], \end{aligned} \tag{67}$$

in which

$$H=\frac{m_1^2}{1+m^2}, L=2(E_1+E_2)\pi\cos 2\pi(t-x)+E_3\sin 2\pi(t-x), A_2=\frac{4\pi^2\epsilon L}{H^{3/2}},$$

$$A_3=\frac{-(n-1)\pi^6\epsilon^3}{2\left(1+\exp(2\sqrt{H}\eta)H^{5/2}\right)}, A_4=L^3\mathrm{sech}^3(\sqrt{H}\eta), L_1=\gamma_1+\gamma_2+2\eta\gamma_1\gamma_2,$$

$$L_2=\frac{2L_5(2H\eta(2+\gamma_2\eta)-\gamma_2\cosh(2\sqrt{H}\eta)-2\sqrt{H}\sinh(2\sqrt{H}\eta))}{H^2},$$

$$\begin{aligned} L_3 = -\gamma_1 - \frac{2L_5\gamma_1(-2H\eta^2+\cosh(2\sqrt{H}\eta)}{H^2} \\ - \frac{4BrL^2\pi^4\epsilon^2\mathrm{sech}(\sqrt{H}\eta)^2(-2\sqrt{H}\eta+\sinh(2\sqrt{H}\eta))}{H^{\frac{3}{2}}}, \end{aligned}$$

$$L_4 = \frac{L_2(1+\gamma_1\eta)+L_3(1+\gamma_2\eta)}{L_1},\ L_5 = BrL^2\pi^4\epsilon^2\mathrm{sech}(\sqrt{H}\eta)^2,$$

$$L_6 = \frac{\mathrm{sech}(\sqrt{H}\eta)^4L^4(n-1)\pi^8\epsilon^4}{8(1+\exp\left(2\sqrt{H}\eta\right))H^3L_1},$$

$$L_7 = \frac{\exp(-4\sqrt{H}\eta)\mathrm{sech}(\sqrt{H}\eta)^4L^4(n-1)(1+\gamma_2\eta)\gamma_1\pi^8\epsilon^4}{(1+\exp(2\sqrt{H}\eta))L_1H^{5/2}},$$

$$H_1 = \frac{Sc}{480M^8\eta^3}\times(60-60M(3+4M)\eta+270M^2\eta^2+480M^3\eta^2+240M^4\eta^2-150M^3\eta^3$$
$$-360M^4\eta^3-240M^5\eta^3-M^4(33+40M(2+M))\eta^4+5M^5(9+4M(7+6M)\eta^5),$$

$$B_1 = \frac{1-M\eta}{2M^2\eta}, B_2 = \frac{1}{2M\eta}, C_1 = \frac{Sc}{480M^8\eta^3}\times(60M-60M^2(3+4M)\eta+210M^3\eta^2$$
$$+480M^4\eta^2+240M^5\eta^2-60M^4\eta^3-240M^5\eta^3(1+M)-M^5(33+40M(2+M))\eta^4),$$

$$C_2 = \frac{Sc}{480M^8\eta^3}\times(30M^2-30M^3(3+4M)\eta+90M^4\eta^2+240M^5\eta^2$$
$$+120M^6\eta^2-30M^5\eta^3-120M^6\eta^3-120M^7\eta^3),$$

$$C_3 = \frac{Sc}{480M^8\eta^3}\times(30M^3-20M^4(3+4M)\eta+30M^5\eta^2+40M^6\eta^2(2+M)),$$

$$C_4 = \frac{Sc}{480M^8\eta^3}\times(15M^4-5M^2(3+4M)\eta, C_5 = \frac{Sc}{160M^3\eta^3}.$$

Results and Discussion

This section is prepared to explore the effects of influential parameters on the temperature, heat transfer coefficient and concentration.

3.1 Temperature profile

Figs. (1–8) are formulated to examine the impact of various involved parameters on temperature distribution θ. Fig. 1 indicates the increasing behavior of temperature profile with wall parameters E_1 and E_2 while E_3 corresponds to reduction in temperature profile. It is in view of the fact that elastic properties of the wall depicted by E_1 and E_2 cause less resistance to flow of fluid velocity as well as energy. On the other hand the damping characteristic of the wall identified by E_3 reduces the velocity and temperature of the fluid (see Fig. 1). The temperature profile is an increasing function of Brinkman number Br (see Fig. 2). This is because of the increase in internal resistance of fluid particles which increases the fluid temperature. The Biot numbers γ_1 and γ_2 on the lower and upper walls have similar effect on the temperature profile *i.e.* increase in γ_1 and γ_2 decreases the temperature profile near upper and lower channel walls respectively (see Figs. 3 and 4). It is seen that increasing γ_1 and γ_2 reduces the thermal conductivity which causes reduction of temperature profile. The Hall parameter m increases the temperature. This is due to the fact that electrical conductivity increases with increasing values of m (see Fig. 5). It is observed from Fig. 6 that Hartman number m_1 lessens the temperature distribution. Also the results drawn in Figs. 7 and 8 show opposite effects of Weissenberg number We and the power law index n *i.e.*, increasing values of We reduces the temperature whereas an increase in n enhances the temperature of fluid. The obtained results are in good agreement with the articles presented in [17–19].

3.2 Heat transfer coefficient

Figs. 9–16 demonstrate the influence of embedded parameters on the heat transfer coefficient Z. The graphs signify the oscillatory behavior of Z because of the propagation of peristaltic waves. Fig. 9 reveals that magnitude of heat transfer coefficient increases for compliant wall parameters E_1, E_2 and E_3. Since E_1, E_2 and E_3 describes the elastic nature of wall that offer less resistance to heat transfer. Increasing values of Brinkman number Br show similar behavior on heat transfer as of wall parameters. However the results obtained are much more distinguished in case of Br (see Fig. 10). The Biot number γ_1 causes reduction in magnitude of heat transfer coefficient on the upper wall. Here thermal conductivity decreases with an increase in γ_1 which lessens the impact of heat transfer coefficient near positive side ($x > -0.1$) as depicted in Fig. 11. Reverse effect of Biot number γ_2 has been observed in the region from Fig. 12 as heat transfer being directly related to Biot number dominates with an increase in γ_2 which in turn increases the heat transfer distribution. Fig. 13 shows decrease in heat transfer coefficient Z with Hall parameter m. Also in absence of Hall parameter ($m = 0$) the results are much more distinguished. The Hartman number m_1 is an increasing function of heat transfer coefficient Z as fluid viscosity decreases with an increase in m_1. The less viscous fluid particles will move through gain of higher kinetic energy that causes rise in transfer of heat (see Fig. 14). The effects of Weissenberg number We are displayed in Fig. 15. The obtained results show increase in transfer of heat when We increases as speed of wave increases with an increase in We that supports the transfer of heat. The increasing values of power law index show decline in heat transfer distribution (see Fig. 16).

3.3 Homogeneous-Heterogeneous reactions effects

Effects of homogeneous and heterogeneous reaction parameters M and K and Schmidt number Sc are displayed in the Figs. 17–19. The results drawn in Fig. 17

illustrates the dual behavior of homogeneous reaction parameter K on the concentration profile. It is observed that concentration increases in the region $x > 0.5$ as in this region increase in K enhances the fluid density hence concentration rises while in the region $x < 0.5$ the concentration decreases because viscosity reduces. On the other hand the heterogeneous reaction parameter M shows the opposite behavior when compared with K *i.e.* it increases along positive side of the coordinate axes $(x < 0)$ (since diffusion reduces with an increase in M and less diffused particles will rise the concentration) and decreases along negative side of coordinate axes $(x > 0)$ (as increase in rate of reaction dominates the decrease in diffusion in this region). It is evident from Figs. 17 and 18 that the concentration distribution of reactants increases from $-\eta$ to η in both cases and after a certain value of η it starts decaying. This critical value of η depends on the strength of homogeneous reaction and it is prominent for increasing K. The effects of Schmidt number Sc are depicted in Fig. 19. The exhibited results are quite similar to Fig. 17. The drawn results follow by the fact that viscosity of fluid increases with an increase in Schmidt number that provides resistance to flow of fluid. The slow moving fluid particles have small molecular vibrations which lessen the concentration of fluid. As Schmidt number defines the ratio of viscous diffusion rate to molecular diffusion rate. Hence increasing values of Sc enhances the viscous diffusion rate for fixed molecular diffusion rate which in turn helps to increase the concentration of fluid (see Fig. 19). The similar findings are reported by Shaw et al. [24].

3.4 Concluding remarks

The present analysis explores the effects of homogeneous and heterogeneous reactions in the peristalsis of Carreau fluid. Such analysis even for viscous fluid is yet not available. The major results of this study are listed below.

- Similar behavior is observed for compliant wall parameters on temperature profile and heat transfer coefficient.
- Temperature is increasing function of Brinkman number and Hall parameter.
- The Biot numbers and Hartman number decrease the temperature of fluid.
- Opposite effects of Weissenberg number We and power law index n are observed on the temperature profile and heat transfer coefficient.
- Concentration of the reactants is more signified in case of homogeneous reaction parameter K than heterogeneous reaction parameter M.

Author Contributions

Conceived and designed the experiments: TH AT HY AA. Performed the experiments: TH AT HY AA. Analyzed the data: TH AT HY AA. Contributed reagents/materials/analysis tools: TH AT HY AA. Wrote the paper: TH AT HY AA.

References

1. **Mekheimer KhS, Salem AM, Zaher AZ** (2014) Peristaltically induced MHD slip flow in a porous medium due to a surface acoustic wavy wall. J Egyp Math Soc 22: 143–151.

2. **Mekheimer KhS** (2008) Effect of the induced magnetic field on peristaltic flow of a couple stress fluid. Phys Lett A 372: 4271–4278.

3. **Abd elmaboud Y** (2012) Influence of induced magnetic field on peristaltic flow in an annulus. Commun Nonlinear Sci Numer Simul 17: 685–698.

4. **Ali N, Hayat T, Wang Y** (2009) MHD peristaltic flow of a third order fluid in an asymmetric channel. Int J Numer Methods in Fluids 64: 992–1013.

5. **Ellahi R** (2013) The effects of MHD and temperature dependent viscosity on the flow of non-Newtonian nanofluid in a pipe: Analytical solutions. Appl Math Model 37: 1451–1467.

6. **Ebaid A** (2014) Remarks on the homotopy perturbation method for the peristaltic flow of Jeffrey fluid with nano-particles in an asymmetric channel. Comp Math Appl DOI: 10.1016/j.camwa.2014.05.008.

7. **Abd-Alla AM, Abo-Dahab SM, Al-Simery RD** (2013) Effect of rotation on peristaltic flow of a micropolar fluid through a porous medium with an external magnetic field. J Mag Mag Materials 348: 33–43.

8. **Yasmin H, Hayat T, Alsaedi A, Alsulami HH** (2014) Peristaltic flow of Johnson-Segalman fluid in an asymmetric channel with convective boundary conditions. Appl Math Mech 35: 697–716.

9. **Mustafa M, Abbasbandy S, Hina S, Hayat T** (2014) Numerical investigation on mixed convective peristaltic flow of fourth grade fluid with Dufour and Soret effects. J Taiwan Inst Chem Eng 45: 308–316.

10. **Hayat T, Yasmin H, Alsaedi A** (2014) Convective heat transfer analysis for peristaltic flow of power-law fluid in a channel. J Braz Soc Mech Sci Eng DOI: 10.1007/s40430-014-0177-4.

11. **Parsa AB, Rashidi MM, Hayat T** (2013) MHD boundary-layer flow over a stretching surface with internal heat generation or absorption. Heat Transfer–Asian Research 42: 500–514.

12. **Abelman S, Momoniat E, Hayat T** (2009) Steady MHD flow of a third grade fluid in a rotating frame and porous space. Nonlinear Analysis: Real World Appl 10: 3322–3328.

13. **Rashidi MM, Ferdows M, Parsa AB, Abelman S** (2014) MHD natural convection with convective surface boundary condition over a flat plate. Abstract and Applied Analysis 2014: 923487 (10 pages).

14. **Merkin JH** (1996) A model for isothermal homogeneous-heterogeneous reactions in boundary-layer flow. Math Comput Model 24: 125–136.

15. **Zhang Y, Shu J, Zhang Y, Yang B** (2013) Homogeneous and heterogeneous reactions of anthracene with selected atmospheric oxidants. J Environmental Sci 25: 1817–1823.

16. **Kameswaran PK, Shaw S, Sibanda P, Murthy PVSN** (2013) Homogeneous–heterogeneous reactions in a nanofluid flow due to a porous stretching sheet. Int J Heat Mass Transfer 57: 465–472.

17. **Riaz A, Ellahi R, Nadeem S** (2014) Peristaltic transport of a Carreau fluid in a compliant rectangular duct. Alexandria Eng J 53: 475–484.

18. **Awais M, Farooq S, Yasmin H, Hayat T, Alsaedi A** (2014) Convective heat transfer analysis for MHD peristaltic flow in an asymmetric channel. Int J Biomath 7: 1450023 (15 pages).

19. **Ellahi R, Bhatti MM, Vafai K** (2014) Effects of heat and mass transfer on peristaltic flow in a non-uniform rectangular duct. Int J Heat Mass Transfer 71: 706–719.

20. **Tripathi D, Bég OA** (2014) A study on peristaltic flow of nanofluids: Application in drug delivery systems. Int J Heat Mass Transfer 70: 61–70.

21. **Mustafa M, Hina S, Hayat T, Alsaedi A** (2012) Influence of wall properties on the peristaltic flow of a nanofluid: Analytic and numerical solutions. Int J Heat Mass Transfer 55: 4871–4877.

22. **Hina S, Hayat T, Alsaedi A** (2013) Slip effects on MHD peristaltic motion with heat and mass transfer. Arab J Sci Eng 39: 593–603.

23. **El Koumy SR, El Barakat SI, Abdelsalam SI** (2012) Hall and porous boundaries effects on peristaltic transport through porous medium of Maxwell model. Transp Porous Med 94: 643–658.

24. **Shaw S, Kameswaran PK, Sibanda P** (2013) Homogeneous-heterogeneous reactions in micropolar fluid flow from a permeable stretching or shrinking sheet in a porous medium. Boundary Value Problems 2013: 77–86.

25. **Hayat T, Saleem N, Ali N** (2010) Effect of induced magnetic field on peristaltic transport of a Carreau fluid. Commun Nonlinear Sci Numer Simul 15: 2407–2423.